J Mater Sci (2022) 57:1850–1862

Computation & theory

The effect of textured surface on graphene wettability and droplet evaporation

S. Y. Misyura[1,*], V. A. Andryushchenko[1], V. S. Morozov[1], and D. V. Smovzh[1]

[1] *Kutateladze Institute of Thermophysics Siberian Branch, Russian Academy of Sciences, 1 Lavrentyev Ave., Novosibirsk, Russia 630090*

Received: 26 September 2021
Accepted: 26 December 2021
Published online: 11 January 2022

ABSTRACT

The influence of a grain orientation and textured surfaces on the droplet evaporation and the graphene coating wettability is investigated. The study of the behavior of water droplets on graphene-coated substrates is important for the development of highly sensitive sensor technologies. The coating of the graphene layer with water leads to changes in charge concentration and electrical conductivity. To date, there are very few studies on the effect of substrate textures and wall heating on water droplets evaporation on a heated graphene coating. The contact angle depends on the ratio of several factors: textures, grain orientation and grain size. In the final stage of evaporation of a water droplet on a hot textured substrate with graphene, a jump in the contact line of the water droplet is observed. The contact angle abruptly increases almost two times. Molecular-dynamic modeling has shown that the wettability depends on the grains orientation and the annealing duration. The measured experimental value of the copper contact angle of 74–76° after annealing corresponds to the simulation results considering the direct proportionality between the contact angle and the amplitude of the first maximum of the density distributions of water molecules in the vicinity of a smooth copper surface.

Introduction

Much attention to graphene is caused by its unique electrical, mechanical and thermophysical properties [1]. Graphene can be effectively used in optoelectronics due to its high transparency and high conductivity [2]. Graphene-based sensors have a very high sensitivity, which allows registering gases and impurities with a very low concentration [3–5]. Graphene-based membrane technologies can have the following applications: the gas separation, the filtration technologies, the water purification and

Handling Editor: N. Ravishankar.

Address correspondence to E-mail: misura@itp.nsc.ru

https://doi.org/10.1007/s10853-021-06853-7

desalination technology [6–9]. The use of graphene oxide membranes is discussed in Ref. [10].

Graphene, unlike many metals, retains greater stability of properties over time. However, the adsorption of water on the graphene surface and the formation of droplets or a film of water lead to a change in the electrical properties and affect the parameters of sensitive sensors. When the graphene monolayer is covered by a water film, an energy gap of 20–30 meV is realized [11]. The hysteresis behavior of the contact angle of a water droplet on graphene coatings has been investigated in Refs. [12, 13]. The wettability properties of graphene change with the time when the material is exposed to the open air, which is associated with the adsorption of aromatic hydrocarbons [14, 15].

The graphene layer wetting transparency changes on substrates made of different materials [16]. Depending on the substrate material, the graphene coating can have both hydrophilic and hydrophobic properties [17]. The wettability (contact angle of the drop) changes with an increase in graphene layers synthesized on the substrate [18, 19]. With an increase in the number of defects, the graphene surface energy is increased, which leads to an increase in hydrophilicity [20].

Wall texturing influences the wettability and the droplet evaporation modes [21, 22]. Molecular modeling of wettability is presented in [16, 23–25].

The simulation is performed for small sizes (usually tens of nanometers), which does not allow assessing the role of important factors in the evaporation of a drop: free convection in the liquid and gas phases, the influence of the Stefan flow and the thermal inertia of the substrate. In nanoscale droplets, the effect of Rayleigh and Marangoni convection on evaporation is excluded. Therefore, experimental studies on the evaporation of large droplets on heated graphene coatings are necessary. The influence of the Marangoni flow on the droplet evaporation has been studied by Hu H. and Larson R.G. [26]. Textures on the substrate surface lead to increased heat and mass transfer and increase the evaporation rate on heated surfaces [27]. The influence of the thermal conductivity of the substrate on the direction of the surface flow of the liquid has been shown by Ristenpart W.D. [28]. Free convection in the drop increases the heat exchange in the drop and increases evaporation [29–32].

The simulation of the sessile droplet evaporation is given in [33, 34]. The evaporation behavior of aqueous solutions differs from the water evaporation. The evaporation rate of solution droplets changes with time [35–37].

A high degree of hydrophobicity can be achieved both by applying a hydrophobic film with low surface energy of the metal surface [38] and by nano-micro texturing the surface [39–41]. The superhydrophobic surfaces with extremely low contact angle hysteresis ($\theta_{CAH} < 4°$), which exhibits excellent self-cleaning behavior by the zinc oxide nanorods, were investigated by Banik M. [42]. Hydrophobic coatings have a wide technical application. The durability of these surfaces is extremely important in practice. However, prolonged contact with water and with various aggressive media leads to defects in coatings and to a change in wettability [43]. The use of graphene will increase the durability of the coating and the constancy of wettability over time.

An analysis of the literature has shown that there are very few studies on the simultaneous influence of several factors (the nature of the substrate grains, the influence of wall textures and heat transfer) on the wettability and evaporation of a water drop on a graphene-coated copper substrate. These studies are of interest for a wide range of both scientific problems and for technical applications of graphene-coated substrates.

Molecular-dynamic modeling of the effect of roughness and crystalline grains on the wettability of the graphene-coated copper

The paper studied the structuring of water molecules in the vicinity of surfaces of smooth and textured copper plates. The crystallographic orientation of the atoms of the copper plates was chosen to be equal to 100. Further, the influence of grain orientation changes on wettability was investigated. The length, width and thickness of the copper plates were equal: forty, forty and ten angstroms, respectively. The thickness of the layer of water molecules was equal to twenty angstroms. An illustration of a textured copper plate and a water layer is shown in Fig. 1.

To establish the qualitative effect of texturing, the surface of the original copper plate was modified, namely three identical solid bands were cut on the

surface of the copper plate. The width and depth of the bands were equal to five and a half angstroms. The length of the bands coincided with the length of the plate and was equal to forty angstroms. Figure 1 is built in the VMD program [44].

Molecular-dynamic modeling of the system under study was performed using the CHARMM software package [45]. The water environment was considered explicitly. At that, the TIP3P water model was used. The system was studied at a temperature of 300 K in the approximation of the canonical ensemble. To determine the degree of hydrophilicity of the surfaces of copper plates, the structuring of water molecules in the vicinity of these plates was studied. For this purpose, the density profiles of water molecules were calculated depending on the distance to the centers of atoms of the surface layer of copper plates. The density was calculated directly using the UCSF Chimera program [46]. In addition, the density was normalized to the average density of water molecules in the accessible volume. The density distributions of water molecules near smooth and textured copper surfaces are shown in Fig. 2.

The distribution of water molecules is directly related to the hydrophilicity of the surface: the greater the hydrophilicity of the surface is, the closer the maxima of the density distribution are located and the greater their amplitude is. Surface texturing leads to the water density redistribution. Thus, some part of the water molecules gets to the bands cut on the surface (Figs. 1 and 2). The distance d is calculated from the centers of the atoms of the surface layer of copper. In addition, changes in the position

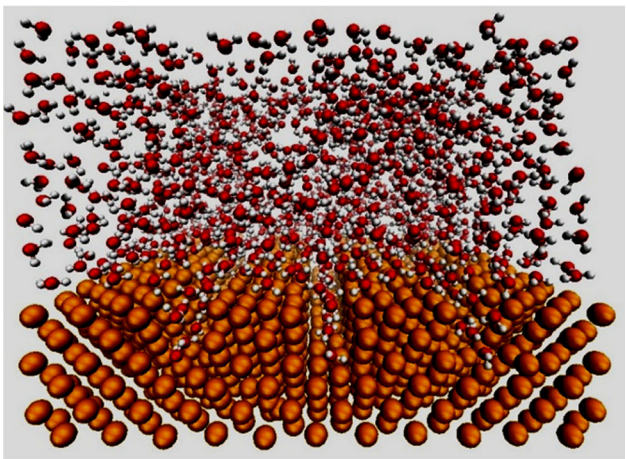

Figure 1 Water molecules in the vicinity of a textured copper plate.

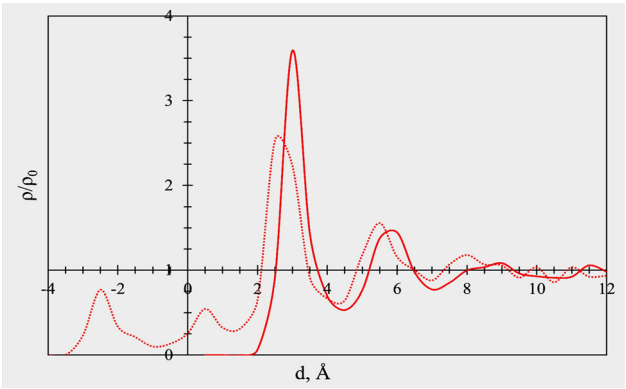

Figure 2 Water density distributions near smooth (solid line) and textured (dotted line) copper surfaces.

and amplitude of the main density maximum are observed. On the one hand, this maximum shifts closer to the surface, which should correspond to an increase in hydrophilicity, and on the other hand, its amplitude decreases, which should correspond to a weakening of hydrophilicity. To determine the degree of hydrophilicity, we calculate the value of m as an integral (Eq. (1)). The integration is carried out by the distance d^* and by the surface area of copper S.

$$m = \int_0^{d^*} \int_0^{S} \rho dSdl. \tag{1}$$

The value m is the mass of water molecules contained in the selected layer dl. Integration is performed from the centers of the surface layer of copper, i.e., 0 to the distance d^*, chosen equal to four angstroms. This value is chosen for the main maximum of the density to fall entirely into the integration region. In addition, at this distance, the values of the distribution densities near the textured and smooth plate practically coincide. As a result, the value of m in the vicinity of the textured surface is about twenty percent higher than the corresponding value for a smooth surface. The surface area of copper due to grooves is about 11% larger than the area of the horizontal surface of the plate (without texturing). Thus, the increase in hydrophilicity (by about 20%) is almost two times as large as the increase in the surface area. The increase in hydrophilicity is not proportional to the increase in the surface area, i.e., it is impossible to increase the intermolecular force and calculate the adhesion (water–solid) only due to the additional growth of the side surfaces of textures. This is because the interaction with the wall increases

in the corners of the grooves. In addition, the molecule inside the groove is affected not only by the interaction with the horizontal wall, but also by the interaction with the two side walls in the groove. The mobility of water molecules can also decrease inside the groove.

Thus, the textured copper surface attracts water more efficiently and, thus, is more hydrophilic. When varying the degree of texturing, we should expect a corresponding change in hydrophilicity, i.e., texturing the surface is potentially one of the possibilities for controlling lyophilicity.

The experimental data presented below show that long-term high-temperature annealing strongly changes the crystal orientation of the grains on the copper surface. Therefore, it is important to consider not only the modeling of molecular interaction on smooth and textured surfaces, but also the influence of grain orientation. The results of modeling the distribution of the density of water molecules (near a copper surface with a single graphene layer) depending on the orientation of the grains are shown in Fig. 3. The blue curve corresponds to orientation of the atoms (111); the green curve corresponds to orientation (110). Figure 3 also shows color images for orientations obtained for smooth and textured surfaces covered with a graphene layer.

In accordance with the simulation, the maximum hydrophilicity corresponds to a smooth copper wall with orientation of atoms (111). The wall textures (after annealing of the substrate) lead to a shift of copper orientation (100) to orientation (110). On the basis of Fig. 4, a copper surface with orientations (110) will have significantly less hydrophilicity than a surface with orientations (111).

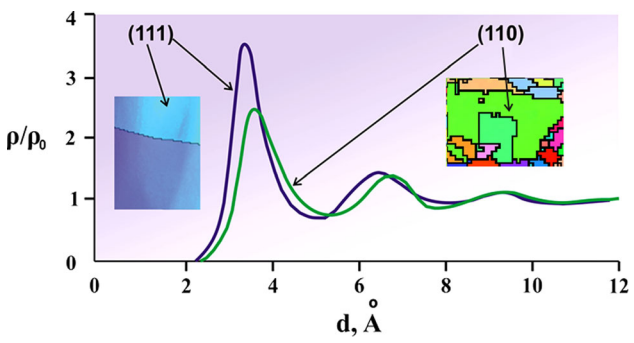

Figure 3 Density distributions of water molecules in the vicinity of a smooth copper surface coated with graphene: the blue curve corresponds to crystallographic orientation of the atoms (111); the green curve corresponds to crystallographic orientation (110).

Assume a direct proportionality between the contact angle and the amplitude of the first maximum (amplitude estimate). Considering the amplitudes (A_m) of the first maxima of the density distribution for the crystallographic orientation (111) and orientation (100) (Fig. 4), we establish that the contact angle of α-copper after annealing (the orientation (111)) should be about 74°. The measured contact angle on α-copper without annealing (the orientation (100)) is 82–84°. Amplitude ratio $A_{m(111)}/A_{m(100)} = 1.1$ (Fig. 4). Then, the static contact angle after annealing (the orientation (111)) is 84°/1.1 = 76°. The measured experimental value is 74–76°, which corresponds to the simulation results. The result obtained confirms the validity of the specified linear relationship. A close value of the contact angle (76°) after the copper annealing with the crystallographic orientation (111) was obtained by Belyaeva [47].

Experimental data and analysis

Experimental methods

The chemical deposition method from the gas phase was used for the synthesis of graphene on a copper substrate. A more detailed description of the method and scheme of the experimental setup for graphene synthesis is given in [48]. The quartz tube furnace was used for the graphene synthesis. This setup was also used for high-temperature annealing of copper in a furnace. Controller maintained the working furnace temperatures with an accuracy of about 1 K. The chromel–alumel thermocouples were used to measure temperatures into the quartz tube. The temperature in the working zone of the reactor during the synthesis of graphene was 1357 K. A mixture of gases of the required concentration was created using a block, which included three flow meters—the bronkhorst regulators. For the graphene synthesis, a polished copper foil (Alfa Aesar 10,950) with the wall thickness of 20 μm was used. The copper composition corresponded to about 99.999%. The copper foil was washed in an aqueous alcohol solution (40%) with the sodium laureth sulfate. The copper foil was washed in distillate, acetone and again in distilled water by the ultrasonic bath. The textures on the foil were created by mechanical processing (pressing). Experimental studies were performed with polished (smooth) copper (Fig. 5a) and with the textured

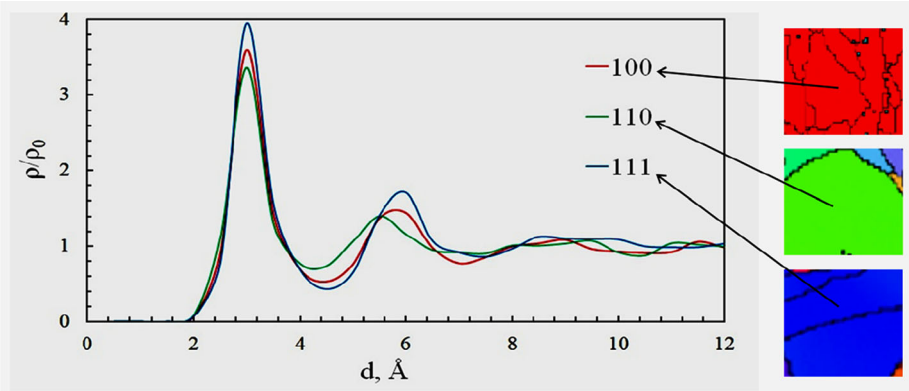

Figure 4 Density distributions of water molecules in the vicinity of a smooth copper surface (without graphene): the blue curve corresponds to crystallographic orientation of the atoms (111); the green curve corresponds to crystallographic orientation (110); the red curve corresponds to the orientation (100).

copper wall (Fig. 5b). The cavity diameter was d_c = 0.2–0.3 mm.

The furnace working chamber was heated to the annealing temperature of about 1343 K. Copper substrates were placed in the quartz tube and then vacuumized up to a gas pressure of about 10^{-2} mbar. After setting the pressure, necessary for the synthesis, the furnace was filled with hydrogen using the hydrogen flow of 5 sccm. Further, the copper substrates were moved to the hot area of the working chamber of the furnace. The hot annealing of copper substrates was carried out in a hydrogen atmosphere.

After the hot annealing, temperatures and compositions of the gas mixture were established for the graphene synthesis using gas composition CH_4/Ar/H_2 (0.22/74/20). The synthesis duration was 10 min after annealing. After the graphene synthesis, the working chamber with graphene samples was removed from the furnace. Then, the obtained samples were cooled with the set rate with a continuous flow of the reaction mixture.

The graphene layer was analyzed by the optical and Raman spectroscopy: Olympus–BX 51 M and LabRam-HR Evolution Raman Spectrometer-JOBIN YVON Technology HORIBA-Scientific. The crystalline grains were analyzed by EBSD method using the Hitachi S 3400 N scanning electron microscope. The measurements have shown that the entire copper surface was covered with 1–2 layers of graphene for both smooth surface and textured copper. The low values of the maxima ratio $I_D/I_G < 0.17$ indicated a good quality of the graphene layer (low defectiveness of the graphene coating was realized) for a smooth and structured surface.

The measuring scheme of the droplet contact angle is shown in Fig. 5c. Degassed distillate was used as a liquid. Droplet was placed on a horizontal copper surface. The average value of the droplet static contact angle was determined from three repeated measurements. The droplet contact angle θ_0 was measured by the tangential method. The electronic dispenser Novus-Thermo Scientific was used to create a drop. The dispenser was located perpendicular

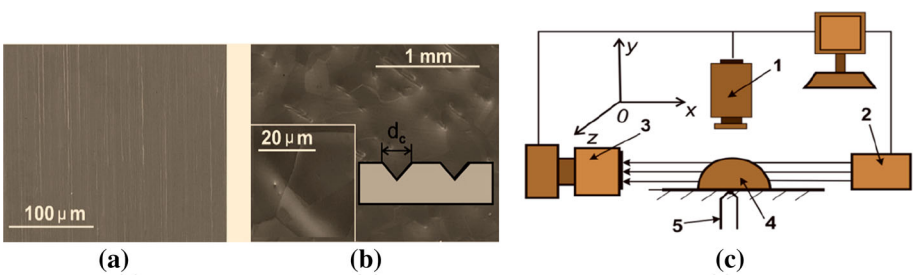

Figure 5 (**a**) Photograph of the smooth surface of copper; (**b**) the textured copper (cavity diameter d_c = 0.2–0.3 mm); (**c**) the measuring scheme of droplet geometric parameters: 1—video camera; 2—source of plane-parallel light; 3—camera (Nikon D-750); 4—water droplet; 5—thermocouple.

to the wall at a distance of 4–5 mm from the wall surface to exclude the droplet breakup after its fall. The process of water squeezing was realized at a constant speed. The repeated measurements demonstrated a match between droplet diameters and droplet contact angles of about 3–4%. Optical system with the plane-parallel lights was used to provide shadow images of a water droplet. The following equipment was used: Source MI-150; Telecentric backlight illuminator 62–760 (Edmund Optics); Glass fiber optics cable-BX4 type Dolan-Jenner; Video camera–FastVideo-500 (Macro lens-Sigma, 105 mm, f/2.8, G IF-ED AF-S 9. The relative measurement error of the droplet contact angle did not exceed 1–2°.

The influence of the hot annealing and wall textures on wettability

The hot annealing is used not only to change the parameters of the crystal grains of the substrate, but also to improve the quality of the graphene coating. The combination of the hot annealing and the mechanical action contributes to an increase in the material strength. However, texturing of the copper substrate can lead to an increase in the graphene defectiveness during its synthesis. It was indicated above (according to the measurement data of the Raman spectroscopy) that the wall textures did not lead to a noticeable increase in the defectiveness of the graphene layer. The kinetics of graphene formation on a copper substrate was shown to depend on the crystal orientation of the grains [48].

The grains crystallographic orientation was controlled by the thermal annealing of copper [49]. The growth rate of graphene layer with grains orientation (1 0 0) was shown to be lower than with orientation (1 1 1). Different rates of graphene growth were associated with different diffusion rates of carbon atoms on crystalline faces [50].

In paragraph 2, the simulation proved that the textures on the wall surface increase the wettability for copper after annealing. Hydrophilicity increases for well-wetted surfaces (Eq. 2),

$$\cos\theta_1 = f\cos\theta \tag{2}$$

where the angle θ refers to a smooth (polished) wall, and the angle θ_1 corresponds to a rough or textured wall. The parameter f takes into account the influence of increased roughness, and f is defined as the ratio of the actual area of the wall surface to the normally projected area. On the other hand, the shift of the grain orientation from (111) to (110) and (100) leads to a noticeable decrease in wettability. Thus, these factors have an inverse (competing) effect on wettability. Depending on the geometry of the textures, the grain size and their orientation (the ratio of the number of grains of different orientations), the use of texturing and high-temperature annealing can lead to both an increase and a drop in the value of the static contact angle of the drop.

Figure 6 presents images of the grain orientation by the EBSD method.

Smooth copper without graphene and without annealing has grain orientation (100). After annealing and synthesis of graphene, the smooth surface shows orientation (111). According to the simulation results, the shift from (100) to (111) leads to an increase in wettability and a decrease in the contact angle of the drop. The textured copper foil after annealing and graphene synthesis has many orientations. The simulation shows that the shift from (100) to (110) leads to a decrease in wettability (an increase in the contact angle). In addition, the contact angle on the graphene coating is determined not only by copper, but also by graphene. Graphene has a neutral wettability (contact angle of 91–92°). It is important to note the following feature of the simultaneous influence of several factors. For smooth copper with orientation (100) or (111), an increase in roughness should lead to an increase in wettability. After the synthesis of graphene on a textured surface with grain orientation (110), the sample can become hydrophobic. In this case, the increase in roughness enhances the hydrophobic properties and increases the droplet contact angle.

The smooth surface roughness was measured with a scanning NanoScan-3D nanohardometer using the atomic force microscopy (AFM) method. Processing data on roughness was carried out using the Gwyddion program. Scanning of the sample surface was performed in semi-contact mode using a diamond tip of the “cube angle” type, which had the following parameters: image size of 94.44 × 108.31 μm; number of scanning points 512 × 512; scanning speed of 10 μm/s with a step of 184.45 nm over X and with a step of 211.54 nm over Y.

High-temperature annealing affects the surface roughness of the substrate and the crystal orientation of the grains, as well as the quality of the synthesized graphene. With an increase in the annealing duration,

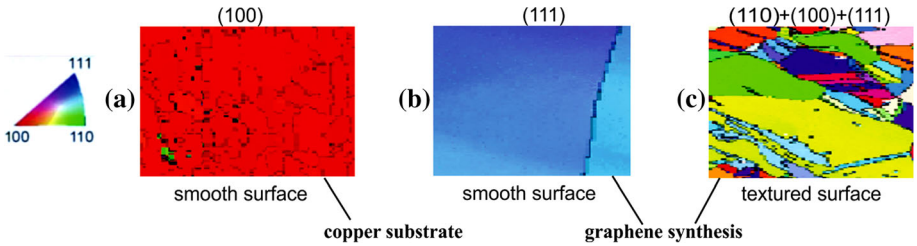

Figure 6 EBSD images: (**a**) smooth copper without graphene; (**b**) smooth copper with graphene; (**c**) textured copper with graphene.

the values of *Ra* and *Rq* decrease, which leads to the more uniform graphene coverage [51]. The concentration of hydrogen during annealing and synthesis of graphene also affects the surface roughness. With an increase in the hydrogen concentration from 0 to 50%, the *Rq* values decrease several times. At a lower initial roughness (before annealing), the effect of hydrogen concentration on the *Rq* values increases [52]. Defects on the substrate surface act on the nucleation behavior during the graphene synthesis [53, 54]. The defects reduce the nucleation barrier for graphene growth.

The 2D AFM images and the roughness profiles of copper foil, as well as images of graphene films are shown in Fig. 7. The roughness of the roughness profiles is obtained without taking into account periodic spatial changes in height (waviness), which are not associated with annealing. Experimental data show that when annealing the foil, the values of *Ra* and *Rq* decrease. Graphene synthesis leads to a certain increase in the values of *Ra* and *Rq* due to the local defectiveness of the graphene layer (Table 1). Literature contains experimental data on both the reduction of the surface roughness of copper and its growth after high-temperature annealing [55], which is probably related to a specific method of foil manufacturing, the method of processing the material before annealing, as well as the duration of annealing. Annealing is also affected by the composition of gases and temperature. It should be noted that the annealing of the foil in the presented work (as opposed to Ref. [51]) was carried out completely in the atmosphere of H_2 (100% H_2). In addition, long-term high-temperature annealing (2 h) was used.

Experimental data on the effect of the thermal annealing duration on the initial contact angle of a water drop are shown in Fig. 8a. The annealing temperature corresponded to 1357 K. All the samples were kept in the air atmosphere for several weeks after annealing. Therefore, the surface of all samples was covered with a layer of adsorbed hydrocarbon impurities. It may be assumed that the influence of the layer of adsorbed hydrocarbons had a qualitatively identical character, i.e., all curves were shifted toward higher values of the contact angle.

As it was mentioned above, changes in the grain orientation for smooth copper lead to a noticeable decrease in the contact angle. Graphene coating and prolonged annealing lead to a shift of Curve 1 toward higher values of the contact angle (Curve 2). A noticeable excess of θ_0 for curve 2 compared to Curve 1 (for long annealing times) may be explained by various effects of hydrocarbon impurities. For copper coated with graphene and a layer of hydrocarbons, the distance δ_2 (between the layer of water and copper molecules) is noticeably greater than the distance δ_1 between water and copper (Fig. 8b). Obviously, due to the strong power dependence of the intermolecular interaction on the distance δ, the wettability for Curve 2 should be worse than for Curve 1. Curve 3 corresponds to the hydrophobic state of the surfaces at any annealing duration. To date, there are no correct models that would take into account the influence of the CHn layer on the total intermolecular interaction. In addition, it is extremely difficult to get rid of the formation of this layer. The easiest way to eliminate the CHn layer is to place sensitive sensors in the atmosphere of purified gases. However, it is difficult to realize selective air purification from hydrocarbon impurities, while maintaining a low concentration of gases (or particles) that a graphene-based sensor should register. The presence of the CHn layer can ensure the constancy of the electrical properties in time, but at that hydrocarbons lead to a decrease in the sensitivity of the sensor and, accordingly, to an increase in the measurement error.

Evaporation of a drop on a heated wall

If we consider small droplets and slow evaporation (when the influence of steam buoyancy, the Stefan flow and free convection can be neglected), then four

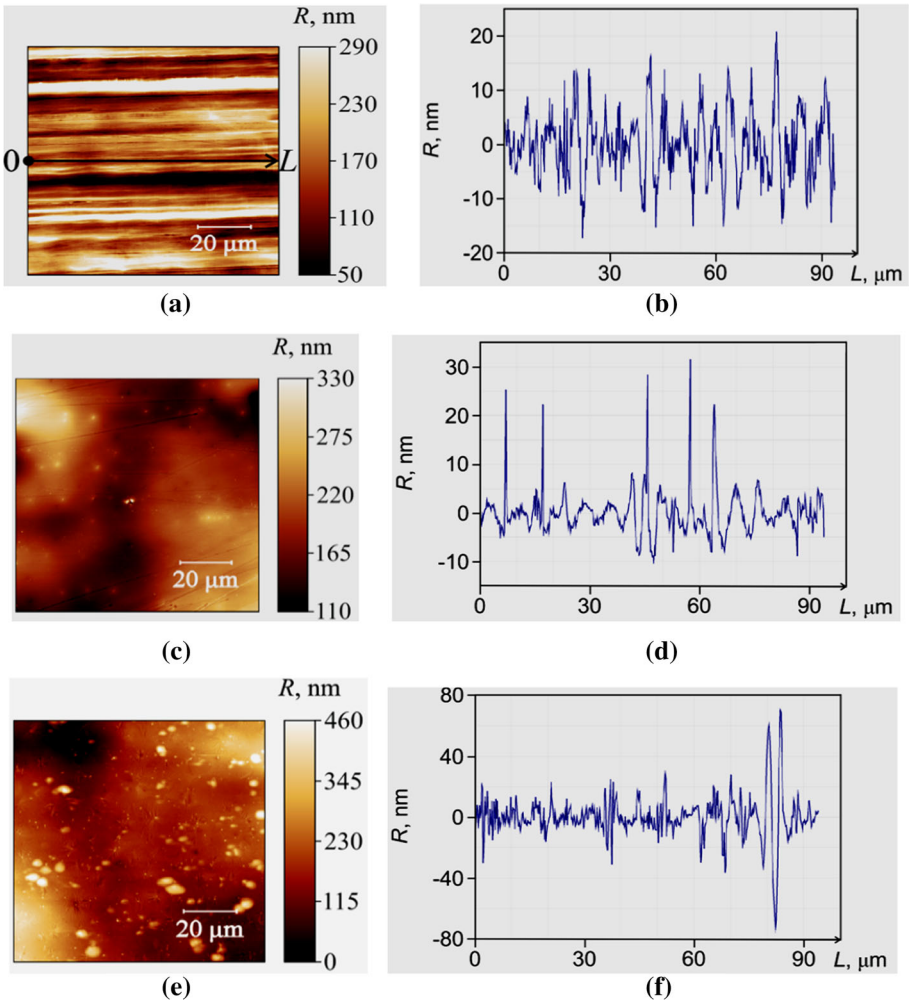

Figure 7 Morphology of the sample surface; (**a, c and e**) 2D AFM image; (**b, d and f**) roughness profiles along 0*L* (**a**): (**a, b**) copper foil without annealing; (**c, d**) copper foil with annealing 2 h; (**e, f**) copper foil with annealing for 2 h and with the graphene synthesis within 10 min.

Table 1 Average values of the roughness profiles along 0*L* (the roughness average, *Ra*); the root mean square roughness, *Rq*)

(nm)	Cooper foil		
	Without annealing	Annealing (2 h)	Annealing (2 h) + graphene synthesis (10 min)
Ra	4.9	3.1	8.5
Rq	6.2	4.5	14.2

characteristic modes of the liquid droplet evaporation are realized: (1) the contact droplet radius (CCR, R = const, θ = var), when the contact droplet angle θ decreases with time; (2) the constant droplet contact angle (CCA, R = var, θ = const), when the droplet diameter decreases with time; (3) both the droplet contact angle and the droplet radius continuously decrease with time (R = var, θ = const); (4) short-term changes are imposed on the CCA or CCR mode: the droplet radius and the droplet contact angle decrease abruptly.

The second mode (the CCA evaporation mode) corresponds to Eq. (3) [33].

$$dV/dt = k(V)^{1/3}, (V/V_0)^{2/3} = 1 - k_1 t \quad (3)$$

where k is the coefficient, which depends on the vapor–air diffusion and on the difference between the equilibrium partial vapor pressure on the droplet surface and the vapor pressure of the external air at a distance from water droplet.

The droplet evaporation in the CCR mode is implemented in accordance with Eq. (4) [34],

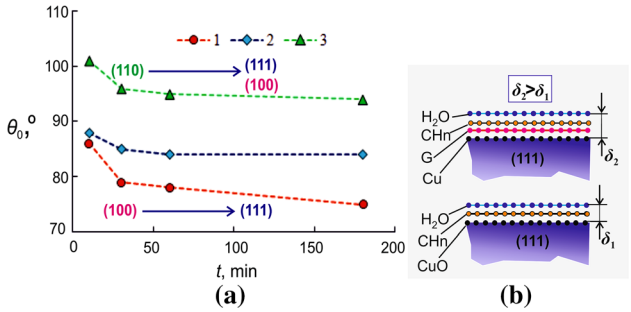

Figure 8 (**a**) Changes in the initial contact angle of the drop depending on duration of the thermal annealing: **1**—smooth copper without graphene; **2**—smooth copper with graphene; **3**—textured copper with graphene; (**b**) multilayer scheme (Cu—copper, G—graphene, CHn—hydrocarbon impurities, H_2O—water).

$$j = \triangle V \rho_l / \triangle t = -rDf(\theta)\rho_l \triangle \rho \tag{4}$$

where the difference in partial pressures of water vapor $\Delta\rho = \rho_s - \rho_a$, ρ_s is the equilibrium water vapor density for droplet free surface, ρ_a is the water vapor density in external air, ρ_l is water density, and D is the diffusion coefficient (water vapor–air). During evaporation in the CCR mode, the droplet volume and the contact angle decrease quasi-linearly with time (Eq. (5)).

$$\theta/\theta_0 \sim 1 - k_1 t^n; V/V_0 \sim 1 - k_2 t^n (n = 1) \tag{5}$$

If a droplet evaporating in the CCA mode, the droplet volume is replaced with the radius, and then we get the ratio in the form of Eq. (6),

$$r/r_0 \sim (1 - k_3 t)^n; (n = 0.5) \tag{6}$$

The peculiarity of this droplet evaporation is that in the initial time period, the droplet contact radius decreases more slowly than for the large time values.

When the third droplet evaporation mode is realized (both the droplet radius and the droplet contact angle change with t), the change in r/r_0 and θ/θ_0 is realized according to Eq. (6) (at $0.5 < n < 1$). Thus, a change in the droplet evaporation mode must also be accompanied by modification of the law of changes in volume, radius and contact angle over time.

Figure 9a shows the experimental data of the droplet volume change with time for smooth and structured walls of the copper foil at a constant wall temperature T_w = 30 °C. At $t < 500$ s, a higher droplet evaporation rate (the average evaporation rate for the specified period of time) corresponds to a smooth wall (the volume curve is located below). At

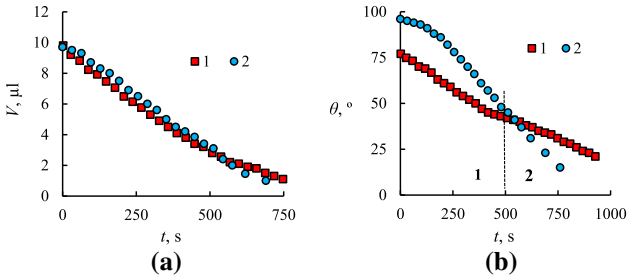

Figure 9 Changes in the droplet parameters with time for copper without graphene coating (surface temperature T_w = 30 °C; annealing time of 2 h; 1—the smooth copper; 2—the textured copper: (**a**) changes in the droplet volume; (**b**) changes in the droplet contact angle.

$t > 500$ s, the droplet evaporation is higher on the textured wall.

The roughness of the textured wall has led to a more stable behavior for the contact line of the drop (Curve 2 in Fig. 9b). With the exception of the initial time section, Curve 2 has a quasi-linear character. For a smooth wall (Curve 1), there are two evaporation modes. For the first mode, there is a quasi-attached contact line of a drop. After t = 500 s (the second mode), the drop radius decreases slightly with time. As a result, the evaporation rate decreases and the slope of the curve θ decreases.

Figure 10 presents the experimental data of changes in the droplet volume, the droplet radius and the droplet contact angle on a copper substrate with a single graphene layer. Curve 1 corresponds to a smooth copper surface with graphene. Curve 2 corresponds to a textured copper with graphene. The initial droplet contact angle is higher for the structured sample (almost by 10°) compared to the smooth sample.

In accordance with Eq. (4), the droplet evaporation rate (j) in the CCR mode is proportional to the droplet radius. The higher the droplet radius r is, the higher the evaporation rate is. Therefore, the evaporation rate for the smooth sample (Curve 1) should be higher than for the textured sample (Curve 2), which corresponds to Fig. 10a. The CCR mode is implemented on a smooth wall in mode 1 (Fig. 10b, c). In mode 2, the contact line partially loses stability. The droplet radius decreases in the CCA mode. Further, in mode 3, evaporation is realized in the mode of constant radius of the drop base (CCR mode). The textured wall increases the stability of the contact line of the drop (Curve 2). The diameter of the drop is

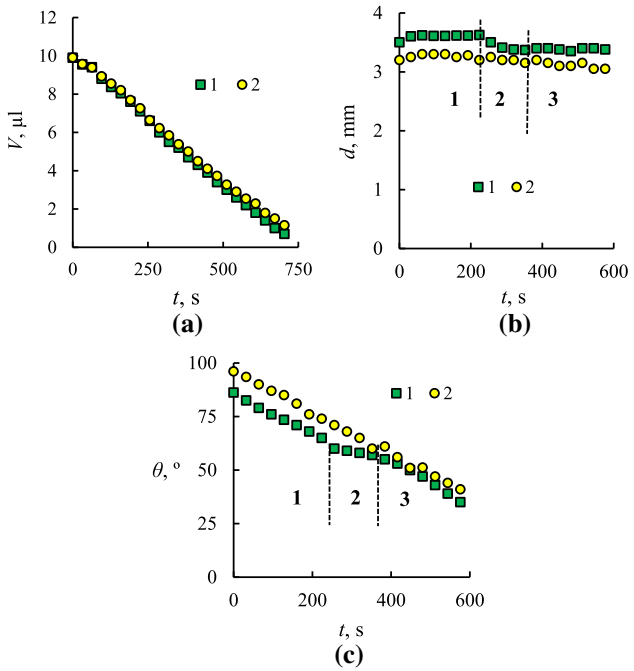

Figure 10 Changes in the parameters of the droplet with time for copper with graphene (the surface temperature T_w = 30 °C; the hot annealing time—2 h; 1—the smooth copper; 2—the textured copper: (**a**) the droplet volume; (**b**) the droplet diameter; (**c**) the droplet contact angle.

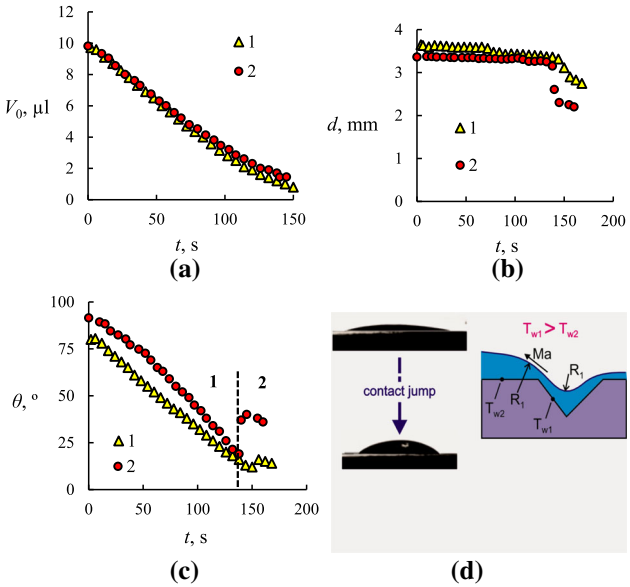

Figure 11 Droplet evaporation over time (the wall temperature T_w = 70 °C; the annealing time—2 h; 1—smooth copper without graphene; 2—structured copper with graphene: (**a**) changes in the drop volume; (**b**) changes in the diameter of the droplet base; (**c**) changes in the droplet contact angle; (**d**) photographs of a sharp change in the shape of a drop and a diagram of the driving forces near the cavity.

quasi-constant in the given time interval $0 < t < 600$ s (Fig. 10b).

The behavior of the contact angle for the textured sample has a quasi-linear character (Fig. 10c). Despite the fact that the textured surface has a greater hydrophobicity (the droplet contact angle θ_0 (for t = 0 s) for sample 2 is 96°, and for the smooth sample θ_0 = 86°), the droplet evaporation on the textured surface is realized in the CCR mode.

Figure 11 shows graphs of the drop evaporation at a constant wall temperature T_w = 70 °C. Curve 1 corresponds to a smooth surface of copper without graphene. Curve 2 is given for structured copper coated with graphene. A higher wettability for smooth copper contributes to a higher evaporation rate (Fig. 11a). In mode 2, the contact line of the drop loses stability. For a structured surface, a strong abrupt increase in the contact angle is observed (Fig. 11c). After the loss of stability, θ increases almost two times and a new state of equilibrium is established (Fig. 11c shows photographs of the abrupt change in the drop profile). Such a strong change in the contact angle may be associated with dynamic and thermal factors. Since the size of the cavity significantly exceeds the height of the precursor film of the drop, there is a liquid film inside the cavity (Fig. 11d). When the drop evaporates, the contact angle decreases. Due to the difference in the curvature of R_1 and R_2, the shape of the drop may change. Due to the difference in temperatures T_{w1} and T_{w2} and due to the gradient of the surface tension of water, the movement of the liquid is realized. The thermocapillary force dramatically reduces the stability of the contact line. In mode 1, the wall textures increase the stability of the contact line (CCR mode), and in mode 2 a jump-like transition to a new equilibrium state is realized.

Conclusions

The combined use of high-temperature annealing, the copper foil surface texturing and the synthesis of graphene allows controlling the wettability of the graphene coating.

The texturing of copper without graphene and the use of annealing significantly increase the hydrophilicity (at long-term annealing, the angle corresponds to 73–76°). The texturing of copper with

graphene leads to the hydrophobicity of the substrate (the contact angle increases to 99–101°). The prolonged annealing decreases the angle to 94–96°.

The long-term hot annealing of the smooth copper with graphene leads to the shift of crystal grain orientation (100) to orientation (111). When texturing copper, several grain orientations are formed.

Molecular-dynamic modeling has shown that the wettability depends both on the textures and on the orientation of the grains and the duration of annealing. These factors can both increase and decrease wettability. As a result, copper substrates with graphene can be both hydrophilic and hydrophobic.

The measured experimental value of the contact angle of 74–76° corresponds to the simulation results considering the direct proportionality between the contact angle and the amplitude of the first maximum of the density distributions of water molecules in the vicinity of a smooth copper surface.

The textured surface of the copper foil shows an abrupt increase in the contact angle of the drop in the final stage of evaporation. After the loss of stability of the contact line of the drop, the contact angle sharply increases almost two times and a new state of equilibrium is established for the contact line.

Combining the surface textures, the graphene coating and the hot annealing allow changing the droplet evaporation modes and controlling the droplet evaporation rate.

Acknowledgements

The studies were carried out within the framework of the state assignment for the IT SB RAS.

Declarations

Conflict of interest The authors declare that they have no conflict of interest.

References

[1] Castro NA, Guinea F, Peres N, Novoselov K, Geim A (2009) The electronic properties of graphene. Rev Mod Phys 81:109–162

[2] Ferrari AC et al (2014) Science and technology roadmap for graphene, related two-dimensional crystals, and hybrid systems. Nanoscale 7:4598–4810

[3] Novikov S, Lebedeva N, Satrapinski A (2015) Ultrasensitive NO_2 gas sensor based on epitaxial graphene. J Sens 5:1–7

[4] Lerner MB et al (2017) Large scale commercial fabrication of high quality graphene-based assays for biomolecule detection. Sens Actuators B 239:1261–1267

[5] Schedin F, Geim AK, Morozov SV, Hill EW, Blake P, Katsnelson MI, Novoselov KS (2007) Detection of individual gas molecules adsorbed on graphene. Nat Mater 6:652–655

[6] Akbari A, Sheath P, Martin ST, Shinde DB, Shaibani M, Banerjee PC, Tkacz R, Bhattacharyya D, Majumder M (2016) Large-area graphene-based nanofiltration membranes by shear alignment of discotic nematic liquid crystals of graphene oxide. Nat Commun 7:1089

[7] Nair RR, Wu HA, Jayaram PN, Grigorieva IV, Geim AK (2012) Unimpeded permeation of water through helium-leak-tight graphene-based membranes. Science 335:442–444

[8] Surwade SP, Smirnov SN, Vlassiouk IV, Unocic RR, Veith GM, Dai S, Mahurin SM (2015) Water desalination using nanoporous single-layer graphene. Nat Nanotechnol 10:459–464

[9] Sun P, Wang K, Zhu H (2016) Recent developments in graphene-based membranes: structure, mass-transport mechanism and potential applications. Adv Mater 28:2287–22310

[10] An D, Yang L, Wang TJ, Liu B (2016) Separation performance of graphene oxide membrane in aqueous solution. Ind Eng Chem Res 55:4803–4810

[11] Ribeiro RM, Peres NMR, Coutinho J, Briddon PR (2008) Inducing energy gaps in monolayer and bilayer graphene: local density approximation calculations. Phys Rev B 78:1–7

[12] Lafkioti M, Krauss B, Lohmann T, Zschieschang U, Klauk H, Klitzing KV, Smet JH (2010) Graphene on a hydrophobic substrate: doping reduction and hysteresis suppression under ambient conditions. Nano Lett 10:1149–1153

[13] Li Z, Wang Y, Kozbial A, Shenoy G, Zhou F, McGinley R et al (2013) Effect of airborne contaminants on the wettability of supported graphene and graphite. Nat Mater 12:925

[14] Aria AI, Kidambi PR, Weatherup RS, Xiao L, Williams JA, Hofmann S (2016) Time evolution of the wettability of supported graphene under ambient air exposure. J Phys Chem C 120:2215–2224

[15] Liu L, Ryu S, Tomasik MR, Stolyarova E, Jung N, Hybertsen MS, Steigerwald ML, Brus LE, Flynn GW (2008) Graphene oxidation: thickness-dependent etching and strong chemical doping. Nano Lett 8:1965–1970

[16] Melios C, Giusca CE, Panchal V, Kazakova O (2018) Water on graphene: review of recent progress. 2D Mater 5:022001

[17] ShihC J, Wang QH, Lin S, Park KC, Jin Z, Strano MS, Blankschtein D (2012) Breakdown in the wetting transparency of graphene. Phys Rev Lett 109:1–5

[18] Ashraf A, Wu Y, Wang MC, Aluru NR, Dastgheib SA, Nam SW (2014) Spectroscopic investigation of the wettability of multilayer graphene using highly ordered pyrolytic graphite as a model material. Langmuir 30:12827–12836

[19] Munz M, Giusca CE, Myers-Ward RL, Gaskill DK, Kazakova O (2015) Thickness-dependent hydrophobicity of epitaxial graphene. ACS Nano 9:8401–8411

[20] Shin YJ, Wang Y, Huang H, Kalon G, Wee ATS, Shen Z, Bhatia CS, Yang H (2010) Surface-energy engineering of graphene. Langmuir 26(6):3798–3802

[21] Misyura SY (2020) Dependence of wettability of microtextured wall on the heat and mass transfer: simple estimates for convection and heat transfer. Int J Mech Sci 170:105353

[22] Misyura SY (2019) The influence of convection on heat transfer in a water layer on a heated structured wall. Int Comm Heat Mass Transf 102(102):14–21

[23] Shih C-J, Strano MS, Blankschtein D (2013) Wetting translucency of graphene. Nat Mater 12:866–869

[24] Huang Y, Jun LJ, Meng S (2018) Transparency in graphene mediated evaporation. 2D Mater 5:041001

[25] Parobek D, Liu H (2015) Wettability of graphene. 2D Mater 2:032001

[26] Hu H, Larson RG (2005) Analysis of the effects of Marangoni stresses on the microflow in an evaporating sessile droplet. Langmuir 21:3972–3980

[27] Misyura SY, Kuznetsov GV, Feoktistov DV, Volkov RS, Morozov VS, Orlova EG (2019) The influence of the surface microtexture on wettability properties and drop evaporation. Surf Coat Technol 375:458–467

[28] Ristenpart WD, Kim PG, Domingues C, Wan J, Stone HA (2007) Influence of substrate conductivity on circulation reversal in evaporating drops. Phys Rev Lett 98:148301

[29] Misyura SY (2018) The influence of characteristic scales of convection on non-isothermal evaporation of a thin liquid layer. Sci Rep 8:11521

[30] Kuznetsov GV, Misyura SY, Volkov RS, Morozov VS (2019) Marangoni flow and free convection during crystallization of a salt solution droplet. Colloids Surf A 572:37–46

[31] Misyura SY, Volkov RS, Filatova AS (2018) Interaction of two drops at different temperatures: the role of thermocapillary convection and surfactant. Colloids Surf A 559:275–283

[32] Misyura SY, Egorov RI, Morozov VS, Zaitsev AS (2021) Emergence and breakup of a cluster of ordered microparticles during the interaction of thermocapillary and thermogravitational convection. Powder Technol 379:165–173

[33] Picknett RG, Bexon R (1977) The evaporation of sessile or pendant drops in still air. J Colloid Interf Sci 61:336–350

[34] Girard F, Antoni M, Sefiane K (2008) On the effect of Marangoni flow on evaporation rates of heated water drops. Langmuir 24:9207–9210

[35] Misyura SY (2015) High temperature nonisothermal desorption in a water-salt droplet. Int J Therm Sci 92:34–43

[36] Misyura SY (2018) The anomalously high rate of crystallization, controlled by crystal forms under the conditions of a limited liquid volume. Cryst Growth Des 18:1327–1338

[37] Egorov RI, Misyura SY, Morozov VS, Zaitsev AS (2021) Self-organization of TiO_2 microparticles on the surface of a thin liquid layer due to local heating and the formation of convective cells. J Mol Liq 324:114685

[38] Hou X, Wang L, Zhou F, Li L (2011) Fabrication of ZnO submicrorod films with water repellency by surface etching and hydrophobic modification. Thin Solid Films 519:7813–7816

[39] Emelyanenko AM, Shagieva FM, Domantovsky AG, Boinovich LB (2015) Nanosecond laser micro- and nanotexturing for the design of a superhydrophobic coating robust against long-term contact with water, cavitation, and abrasion. Appl Surf Sci 332:513–517

[40] Boinovich LB, Emelyanenko AM, Modestov AD, Domantovsky AG, Emelyanenko KA (2017) Not simply repel water: the diversified nature of corrosion protection by superhydrophobic coating. Mendeleev Commun 27:254–256

[41] Boinovich LB, Emelyanenko AM, Emelyanenko KA, Modin EB (2019) Modus operandi of protective and anti-icing mechanisms underlying the design of longstanding outdoor icephobic coatings. ACS Nano 13:4335–4346

[42] Banik M, Chakrabarty P, Das A, Ray SK, Mukherjee R (2019) Colloidal transfer printing–mediated fabrication of zinc oxide nanorods for self-cleaning applications. Adv Mater Interfaces 6:1900063

[43] Varughese SM, Bhandaru N (2020) Durability of submerged hydrophobic surfaces. Soft Matter 16:1692–1701

[44] Humphrey W, Dalke A, Schulten K (1996) VMD: visual molecular dynamics. J Mol Gr 14:33–38

[45] Brooks B et al (2009) CHARMM: the biomolecular simulation program. J Comput Chem 30:1545–1614

[46] Pettersen EF et al (2004) UCSF Chimera visualization system for exploratory research and analysis. J Comput Chem 25:1605–1612

[47] Belyaeva LA, Tang C, Juurlink L, Schneider GF (2020) Macroscopic and microscopic wettability of graphene. Langmuir 37:4049–4055

[48] Boyko EV, Kostogrud IA, Bezrukov IA, Krivenko AS, Smovzh DV (2019) The influence of the crystallographic orientation of the copper catalytic substrate crystallites on the mechanical transfer of graphene. Mater Res Express 6:125628

[49] Hu J, Xu J, Zhao Y, Shi L, Li Q, Liu F, Ullah Z, Li W, Guo Y, Liu L (2017) Roles of oxygen and hydrogen in crystal orientation transition of copper foils for high-quality graphene growth. Sci Rep 7:45358

[50] Frank O, Vejpravova J, Holy V, Kavan L, Kalbac M (2014) Interaction between graphene and copper substrate: the role of lattice orientation. Carbon 68:440

[51] Shah S, Chiou YC, Lai CY, Apostoleris H, Rahman MM, Younes H, Almansouri I, Ghaferi AA, Chiesa M (2017) Impact of short duration, high-flow H2 annealing on graphene synthesis and surface morphology with high spatial resolution assessment of coverage. Carbon 125:318–326

[52] Akhtar S, Laoui T, Ibrahim A, Kumar AM, Ahmed J, Toor I-ul-H (2019) Few-layer graphene film and copper surface morphology for improved corrosion protection of copper. JMEPEG 28:5541–5550

[53] Wang B, Zhang H-R, Zhang Y-H, Chen Z-Y, Jin Z, Liu X-Y, Hu L-Z, Yu G-H (2014) Effect of Cu substrate roughness on growth of graphene domains at atmospheric pressure. Mater Lett 131:138–140

[54] Wang H, Wang G, Bao P, Yang P, Zhu W, Xie X, Zhang W-J (2012) Controllable synthesis of submillimeter single-crystal monolayer graphene domains on copper foil by suppressing nucleation. J Am Chem Soc 134:3627–3630

[55] Ibrahim A, Akhtar S, Atieh M, Karnik R, Laoui T (2015) Effects of annealing on copper substrate surface morphology and graphene growth by chemical vapor deposition. Carbon 94:369–377